#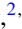 Genuine tripartite nonlocality for random measurements in Greenberger-Horne-Zeilinger-class states and its experimental test

Artur Barasiński [1,2,*] Antonín Černoch,[2,†] Karel Lemr,[2,‡] and Jan Soubusta [2,§]

[1]*Institute of Theoretical Physics, Uniwersity of Wroclaw, Plac Maxa Borna 9, 50-204 Wrocław, Poland*
[2]*Regional Centre of Advanced Technologies and Materials, Joint Laboratory of Optics of Palacký University and Institute of Physics AS CR, Faculty of Science, Palacký University, 17. Listopadu 12, 771 46 Olomouc, Czech Republic*

We present a comprehensive numerical analysis of violations of local realism by tripartite generalized Greenberger-Horne-Zeilinger states. As an indicator of nonlocality we use the nonlocal fraction which describes the probability of violation of local realism under randomly sampled observables. We compare two kinds of local realism based on standard and hybrid local–nonlocal models. As a result, we show a great disproportion of the results determined for both models. Although the nonlocal fraction for standard local realism and tripartite generalized Greenberger-Horne-Zeilinger states significantly increases compared to the bipartite Clauser-Horne-Shimony-Holt scenario, the genuine tripartite nonlocality (the strongest form of nonlocal correlations) is observed with probability much smaller than its bipartite counterpart. Furthermore, when the effects of decoherence on these states are introduced, such disproportion becomes significantly greater. Finally, we present the statistical relevance of various classes of tight Bell inequalities as they are of paramount importance for practical experimental investigation of all problems discussed in this paper. We also propose the nonlocal fraction of hybrid local–nonlocal realism as a measure of genuine tripartite entanglement.

I. INTRODUCTION

Local measurements performed on entangled composite quantum system may yield correlations that are inconsistent with any locally causal description [1]. Such measurement statistics are commonly referred to as nonlocal and recognized as a resource for various quantum information tasks [2] such as quantum key distribution [3–5] or quantum randomness generation [6].

The presence of nonlocality certifies the presence of entanglement in the underlying quantum system without any further assumption or modeling of the experimental setup. However, nonlocal correlations are not solely a consequence of entanglement, but also depend on the choice of measurements. Therefore, the exact relation between entanglement and nonlocality is unknown. For instance, it is unclear whether an increase of entanglement should indicate an increase of nonlocality and so whether the maximally entangled state should also guarantee the maximum of nonlocality. Consequently, what is a good quantifier of nonlocal correlations is still in dispute [7].

The presence of nonlocality is usually revealed by a violation of various Bell inequalities and the degree of such violation (hereafter the strength of violation) is thought of as a measure of nonlocality [1,2]. This kind of demonstra-

tion typically employs carefully chosen measurements whose implementation requires the spatially separated observers to share a complete reference frame [8]. Moreover, it was shown that the maximal quantum violation of certain Bell inequalities crucially requires partial entanglement [9]. The authors of Ref. [7] found this inequivalence between entanglement and strength of violation to be an anomaly. In our paper, we adopted this term to maintain continuity with previous research in this field.

Another interesting possibility to quantify the nonlocality of complex states is based on the probability that random measurements generate nonlocal statistics. In this approach, the following quantity is considered [10,11]:

$$p_V(\rho) = \int f(\rho, \Omega) d\Omega, \qquad (1)$$

where we integrate over a space of measurement parameters Ω according to the Haar measure. The function $f(\rho, \Omega)$ is an indicator function that takes the value 1 whenever the generated behavior is nonlocal and 0 otherwise. Note that with proper normalization the quantity p_V can be interpreted as a probability of violation of local realism. To avoid confusion, we prefer to use the unique term of nonlocal fraction to describe this quantity [12]. It is said that a state ρ_1 is more nonlocal than ρ_2 if $p_V(\rho_1) > p_V(\rho_2)$.

Recently, an intensive theoretical effort has been devoted to study the nonlocal fraction [12–16], showing, for instance, the disappearance of the anomaly between the maximally entangled and maximally nonlocal states. In other words, an increase of entanglement implies the growth of nonlocality measured by p_V and hence the anomaly appears only as an

*artur.barasinski@uwr.edu.pl
†antonin.cernoch@upol.cz
‡k.lemr@upol.cz
§jan.soubusta@upol.cz

artifact of the measure that was used [12,14]. On the other hand, the nonlocal fraction was used to witness entanglement. It was shown that p_V rapidly tends to unity as the number of the parties increases [10,11] and so, p_V provides an effective and experimentally friendly method to detect entanglement in the multiqubit case. However, all of these tests were designed to rule out the so-called standard local realistic models (hereafter the standard model). These purely classical models do not allow for any nonlocal correlation at all and hence in the case of a multipartite system, any two observers are prohibited to share nonlocal correlations. Consequently, the results presented in Refs. [10,11] refer to the distinction between entangled and separable states without distinguishing specific types of multipartite entanglement. The authors of Ref. [14] showed that whenever the nonlocal fraction considering standard local realism with two measurement settings per party is greater than $2(\pi - 3) \approx 28.318\%$, a state cannot be expressed as a convex combination of bipartite entangled states. The cases of $p_V \leqslant 2(\pi - 3)$ are designated as inconclusive. For this reason, it is valuable to analyze this problem more deeply.

It is known that multipartite scenarios offer a much richer and more complex source of correlations (including entanglement and nonlocality) than the bipartite one. Such correlations have already been proven useful for several quantum information tasks [17–19]. Specifically, for more than two observers it is possible to have a hybrid local–nonlocal realistic model (henceforth the hybrid model) that, given a set of projective measurements, permits the existence of nonlocal correlations within subsets of observers while there are local correlations across these subsets [20]. The quantum-mechanical description of nature provides for the existence of correlations that cannot be explained by such a hybrid model. These correlations constitute what is known to be a genuine multipartite (or n way) nonlocality, where all parties are required to be nonlocally correlated [21,22]. The presence of genuine multipartite nonlocality entails the genuine tripartite entanglement [22,23]. Assuming that p_V is a better (or at least alternative) measure of nonlocality [12] than the strength of violation, several important questions arise. (i) What is the nonlocal fraction in the hybrid model? (ii) How it is related to p_V in the standard models? (iii) Is the mutual relation of the nonlocal fraction for the standard and hybrid models correlated to the relationship between the strength of violation for these models? (iv) Can we use the nonlocal fraction of the hybrid model for the experimental detection (quantification) of genuine multipartite entanglement? To the best of our knowledge, none of these questions has been answered yet.

In this work, we concentrate on these problems and analyze the genuine multipartite nonlocality measured by the nonlocal fraction considering local realism under random measurements and its relation with multipartite entanglement and the strength of violation. We focus on generalized Greenberger-Horne-Zeilinger (gGHZ) states as representative members of one of the most important families of quantum states, characterized only by the genuine multipartite entanglement without the bipartite one. These states are therefore a quite natural choice for our investigations. Moreover, it is known that apart from the simplest Clauser-Horne-Shimony-Holt (CHSH) case [24], the nonlocal correlations of multipartite state are described by several inequivalent families of Bell inequalities.

To dispense with the choice of a particular inequality *a priori*, we consider all possible tight Bell inequalities of both models of nonlocality. In contrast to Ref. [14], we adapt the method to work with the correlation coefficients instead of using a linear programming approach. The advantage of such a procedure is its direct experimental implementation, which can be useful for entanglement detection [10,11]. The drawback, however, is a large number of Bell-type inequalities which should be considered in a given Bell scenario. For instance, in the tripartite case with binary inputs and outcomes the complete description of standard and genuine nonlocal correlations requires more than 450 000 Bell inequalities and this value grows exponentially with the number of parties [25,26]. This is the reason why our investigations are limited to the tripartite scenario. Furthermore, by admixing the gGHZ states with white noise we investigate the robustness of the above-mentioned results in an experimentally realistic scenario. We discuss the ability of the experimental measure of p_V in several currently developed setups [27–30]. Finally, we present experimental verification of our predictions.

II. DESCRIPTION OF THE METHOD

In the standard tripartite Bell scenario, the observers Alice (A), Bob (B), and Charlie (C) share entangled systems and each performs local measurements on its shares in spatially separate laboratories. At first, each participant chooses or receives their own independent set of two dichotomic measurements. This corresponds to defining two measurement bases that we label $x, y, z \in \{0, 1\}$ for Alice, Bob, and Charlie, respectively. The measurement in each basis provides each observer with one out of *two* possible outcomes, denoted $a, b, c \in \{0, 1\}$, respectively. Formally, these local dichotomic measurements can be described by a set of orthogonal projectors

$$\{\hat{O}_{a|x}^A, \hat{O}_{b|y}^B, \hat{O}_{c|z}^C\}, \tag{2}$$

where $\hat{O}_{a|x}^A = U_{A,x}^\dagger |a\rangle\langle a| U_{A,x}$ and likewise for other projectors. Here $|a\rangle$ stands for Alice's computational basis state and $U_{A,x}$ denotes a unitary single-qubit transformation parameterized by three angles

$$U_{A,x}(\phi_x^A, \gamma_x^A, \chi_x^A) = \begin{pmatrix} \cos\phi_x^A\, e^{i\gamma_x^A} & \sin\phi_x^A\, e^{i\chi_x^A} \\ -\sin\phi_x^A\, e^{-i\chi_x^A} & \cos\phi_x^A\, e^{-i\gamma_x^A} \end{pmatrix}. \tag{3}$$

In other words, each party starts by fixing two sets of angles ϕ_i, γ_i, and χ_i, thus choosing its two local measurement bases that are subsequently being used throughout the Bell experiment. Even though these angles are continuous quantities, preselecting two sets of angles per party yields a discrete number of possible measurements $\{\hat{O}_{a|x}^A, \hat{O}_{b|y}^B, \hat{O}_{c|z}^C\}$ ($3 \times 2 \times 2 = 12$ in this case) as investigated below.

Following the standard terminology, the corresponding Bell experiment is then fully characterized by the set of joint conditional probability distributions $\mathbf{P} = \{P(abc|xyz)\}$, given by $P(abc|xyz) = \text{Tr}\{\hat{O}_{a|x} \otimes \hat{O}_{b|y} \otimes \hat{O}_{c|z} \cdot \rho\}$, where ρ is a normalized quantum state.

The standard local realistic model is based on the assumption of the existence of a probability distribution $q(\lambda)$ such
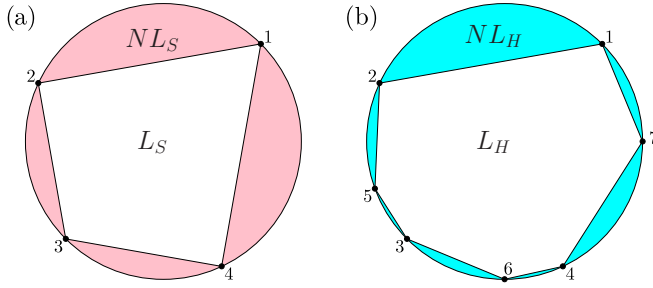
FIG. 1. A schematic representation of the space of quantum correlations. Local correlations form two polytopes denoted by L_S and L_H with respect to standard and hybrid models, respectively. Correlations falling outside L_S (L_H) are called nonlocal with respect to standard (hybrid) model and belongs to NL_S (NL_H). Bell inequalities are the facets represented by straight lines.

that

$$P(abc|xyz) = \sum_{\lambda} q(\lambda) P_\lambda(a|x) P_\lambda(b|y) P_\lambda(c|z), \quad (4)$$

the set of local correlation $P(abc|xyz)$ (denoted as L_S) is convex with finitely many vertices and called the local polytope [31]. The L_S polytop is bounded by 53 856 facets (hyperplanes) [32–34]. Each facet can be described by a linear function of the probabilities $I^{L_S}(\mathbf{P}) \equiv \sum_{abc,xyz} g_{abc}^{xyz} P(abc|xyz) = C_{\text{LHV}}$, where g_{abc}^{xyz} are real coefficients and we assume $C_{\text{LHV}} \equiv 1$ since one can always rewrite $I(\mathbf{P})$ in terms of $g_{abc}^{xyz}/C_{\text{LHV}}$. Correlations which do not admit the above decomposition are referred to as nonlocal and lie outside the local polytope L_S. In other words, they must violate at least one inequality $I^{L_S}(\mathbf{P}) \leqslant 1$. Such an inequality is called the tight Bell inequality and $C_{\text{LHV}} \equiv 1$ depicts the upper threshold of one inequality for the standard local realism [33]. To simplify our notation, henceforth by NL_S, we denote the set of probability distributions $P(abc|xyz)$ which are nonlocal by the mean of standard model, i.e., NL_S is the complement of L_S as shown in Fig. 1(a).

The standard definition of nonlocality and resulting Bell inequalities, however, do not cover all possible variants of tripartite nonlocal correlations. For that reason, one can relax the locality assumption, where pairs of parties are now allowed to group together and share nonlocal resources. In consequence, by L_H we denote the set of tripartite probability correlations admitting the hybrid local–nonlocal decomposition

$$P(abc|xyz) = \sum_{i=1}^{3} \sum_{\lambda_i} q(\lambda_i) P_{\lambda_i}(\delta_i|\beta_i) P_{\lambda_i}(\delta_j\delta_k|\beta_j\beta_k), \quad (5)$$

where $\{i, j, k\}$ is an even permutation of $\{1, 2, 3\}$, $\delta = \{a, b, c\}$, and $\beta = \{x, y, z\}$ as before. In analogy to the previous paragraph, the boundaries of L_H set are given by 405 056 tight Bell inequalities $I^{L_H}(\mathbf{P}) \leqslant 1$ derived by Bancel *et al.* [22]. The probability distributions $P(abc|xyz)$ cannot be decomposed in the hybrid local–nonlocal form, and hence provide a violation of any $I^{L_H} \leqslant 1$, are named genuine tripartite nonlocal and denoted as NL_H [Fig. 1(b)].

An alternative parametrization of $I^{L_S}(\mathbf{P})$ and $I^{L_H}(\mathbf{P})$ is provided by 26 correlation coefficients $\{\langle A_x \rangle, \langle B_y \rangle, \langle C_z \rangle, \langle A_x B_y \rangle, \langle A_x C_z \rangle, \langle B_y C_z \rangle, \langle A_x B_y C_z \rangle\}$ for all

$x, y, z \in \{0, 1\}$, which satisfy the relation $P(abc|xyz) = \frac{1}{8} [1 + (-1)^a \langle A_x \rangle + (-1)^b \langle B_y \rangle + (-1)^c \langle C_z \rangle + (-1)^{a+b} \langle A_x B_y \rangle + (-1)^{a+c} \langle A_x C_z \rangle + (-1)^{b+c} \langle B_y C_z \rangle + (-1)^{a+b+c} \langle A_x B_y C_z \rangle]$. This is the parametrization used in Refs. [22,33]. It is worth mentioning that all correlation coefficients can be measured experimentally. For instance, in the case of the experimental setup based on correlated photons, the correlation coefficients can be expressed as a function of coincidence counts measured on the detectors [30] (discussed later).

The aim of our method is to find, for the gGHZ state,

$$|\theta\rangle = \cos\theta |000\rangle_{ABC} + \sin\theta |111\rangle_{ABC} \quad (6)$$

with $0 \leqslant \theta \leqslant \frac{\pi}{4}$ and a set of observables $\{\hat{O}_{a|x}, \hat{O}_{b|y}, \hat{O}_{c|z}\}$, whether the local realistic model exists and so whether all Bell inequalities $I^{L_S} \leqslant 1$ and $I^{L_H} \leqslant 1$ are satisfied. If even one of I^{L_S} or I^{L_H} is violated then the state is standard nonlocal or genuine nonlocal, respectively [22,33]. We calculate how many sets of settings (in percents) lead to the violation of local realism [see Eq. (1)]. To simplify our notation, by $p_V(NL_S) \equiv p_V^{NL_S}(|\theta\rangle)$ we describe the nonlocal fraction considering standard local realism for the gGHZ state and likewise for $p_V(NL_H)$. In other words, $p_V(NL_S)$ corresponds to the probability that the state $|\theta\rangle$ is standard nonlocal under random measurements.

We stress that the only analytical result on tight inequalities was obtained in Ref. [10] for the simplest scenario of two settings and two outcomes. Naturally, due to the significantly larger number of Bell inequalities appearing in the tripartite case, we see no possibility to make a similar calculation. Instead, we use a numerical approach to integrate over a space of measurement parameters. The measurement operators are sampled according to the Haar measure [35]. The angles γ_i and χ_i are taken from uniform distributions on the intervals: $0 \leqslant \gamma_i, \chi_i \leqslant 2\pi$. To generate ϕ_i in interval $0 \leqslant \phi_i \leqslant \pi/2$ it is convenient to use an auxiliary random variable ξ_i distributed uniformly on $0 \leqslant \xi_i < 1$ and $\phi_i = \arcsin(\sqrt{\xi_i})$. Of course, all variables are generated independently for each observer, measurement, and outcome. The theoretical calculations discussed in this paper have been performed for 10^9 randomly chosen settings.

III. RESULTS AND DISCUSSION

A. Nonlocal fraction: Noiseless scenario

We start by investigating the most ideal scenario: a pure gGHZ state. The particular instance of $\theta = 45°$ was previously analyzed in the context of the standard model. In that case, our result of $p_V(NL_S) \approx 74.688\%$ is consistent with calculations based on linear programming [10,11,14]. As we see in Table I, this value is significantly higher than the nonlocal fraction for the hybrid model, where $p_V(NL_H)$ is around 11.580%. For other values of θ such an observation is also valid and the nonlocal fraction $p_V(NL_S)$ exceeds $p_V(NL_H)$ (see Fig. 2). Naturally, this is not surprising. The definition of local realism admits, if there exists a set of observables which provides factorization (4), than the hybrid nonlocal-local decomposition (5) is also possible but not vice versa. Consequently, the probabilities that the standard and hybrid models exist under randomly chosen measurements

TABLE I. Nonlocal fraction p_V observed for the gGHZ state in Eq. (6) and random measurement settings. The second and third columns corresponds to the nonlocal fraction within standard and hybrid models, respectively. Columns no. 4 to 6 denote various subsets of the hybrid local–nonlocal realism (see the main text).

θ	$p_V(NL_S)$	$p_V(NL_H)$	$p_V(NL_H|T)$	$p_V(T|S_v)$	$p_V(S_v)$
45.00	74.688	11.580	6.309	4.735	0.535
42.63	74.564	11.507	6.299	4.695	0.513
40.26	74.251	11.297	6.285	4.567	0.445
37.89	73.675	10.945	6.222	4.374	0.349
35.53	72.885	10.413	6.052	4.121	0.240
33.16	71.758	9.701	5.722	3.840	0.139
30.79	70.286	8.836	5.214	3.558	0.063
28.42	68.241	7.850	4.564	3.267	0.019
26.05	65.655	6.783	3.817	2.964	0.002
23.68	62.226	5.708	3.053	2.655	1.7×10^{-5}
21.32	57.959	4.682	2.334	2.348	0.0
18.95	52.695	3.713	1.692	2.022	0.0
16.58	46.382	2.843	1.164	1.679	0.0
14.21	39.190	2.078	0.757	1.321	0.0
11.84	31.196	1.423	0.463	0.960	0.0
9.47	22.889	0.878	0.255	0.623	0.0
7.11	14.604	0.455	0.118	0.337	0.0
4.74	6.666	0.161	0.036	0.126	0.0
2.37	0.731	0.018	0.004	0.014	0.0

fulfill the relation $p_V(L_S) = 1 - p_V(NL_S) \leqslant p_V(L_H) = 1 - p_V(NL_H)$ and hence, $p_V(NL_S) \geqslant p_V(NL_H)$. However, the exact value of $p_V(NL_H)$ and the ratio $p_V(NL_S)/p_V(NL_H)$ are not straightforward. (i) The nonlocal fraction $p_V(NL_H)$ for the three-qubit GHZ state is about 2.5 times smaller than the result achieved for the two-qubit GHZ state, i.e., 28.318 % [10]. It
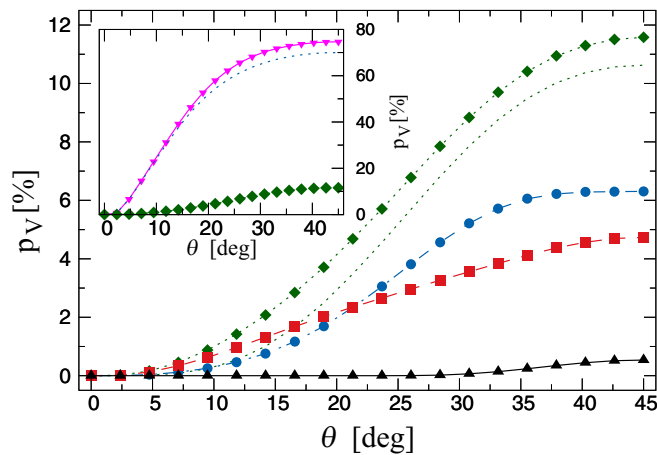

FIG. 2. Nonlocal fraction for the gGHZ state vs θ. The green line with diamond symbols represents the probability of detection of genuine tripartite nonlocality [$p_V(NL_H)$], the blue line with circuit symbols denotes $p_V(NL_H|T)$, the red line with square symbols corresponds to $p_V(T|S_v)$, and the black line with triangle symbols is related to $p_V(S_v)$. The green dotted line corresponds to $p_V(I_4^{L_H})$. The inset shows the mutual relations between $p_V(NL_S)$ (reversed triangle symbols) and $p_V(NL_H)$ (diamond symbols). Finally the blue dashed line represents $p_V(I_4^{L_S})$.

is very interesting since both states are maximally entangled in the two- and three-qubit sense. Assuming p_V to be a measure of nonlocality, one can say that the genuine tripartite nonlocality is much weaker than its bipartite counterpart. (ii) For the GHZ state the ratio $p_V(NL_S)/p_V(NL_H) \approx 6.45$ and could be even higher when $\theta < 45°$. Consequently, the degree of genuine tripartite nonlocality decreases much faster with θ than for standard nonlocality. Interestingly, an opposite conclusion can be found when the strength of violation is taken as a measure of nonlocality. Specifically, for gGHZ states and the standard model the strength of violation is provided either by the 2nd or 15th facet Bell inequality (see Appendix A) while in the hybrid case, one should take the 10th, 96th, or 185th facet inequality [30]. Then it is easy to verify that the ratio $\max(I^{L_S})/\max(I^{L_H}) = \sqrt{2}$ when $29.45° < \theta \leqslant 45°$ and it decreases with decreasing θ. In other words, the relation between the strength of violation of both models of nonlocality either remains constant or the standard nonlocality decreases faster (with θ) than the genuine tripartite one.

Further analysis of p_V also reveals that not every Bell inequality is equivalently important, which yields several important consequences. Specifically, for states $|\theta\rangle$ there are two classes of Bell inequalities which play a dominant role, namely, the 4th facet inequality given in Ref. [33] (hereafter $I_4^{L_S}$) and the 4th facet inequality determined by Bancal *et al.* [22] (denoted as $I_4^{L_H}$). As we see in Fig. 2, these two classes lead to results very close to the exact outcomes for $p_V(NL_S)$ and $p_V(NL_H)$ in the entire range of angles θ. The appropriate relation is written as

$$p_V(NL_S) = p_V(I_4^{L_S}) + \mathcal{O}_4^{L_S},$$
$$p_V(NL_H) = p_V(I_4^{L_H}) + \mathcal{O}_4^{L_H}, \qquad (7)$$

where $p_V(I_4^{L_S})$ and $p_V(I_4^{L_H})$ denote the probabilities of violation for fixed Bell inequality $I_4^{L_S} \leqslant 1$ and $I_4^{L_H} \leqslant 1$, respectively, $\mathcal{O}_4^{L_S}/p_V(NL_S) < 0.06$, and $\mathcal{O}_4^{L_H}/p_V(NL_H) < 0.09$ for all θ (see Appendix B: Tables II and III).

As we have no analytical expression for p_V, the error functions remain unknown and they can be only approximated, for instance, as $\mathcal{O}_4^{L_S} = 0.071 p_V(I_4^{L_S})$ and $\mathcal{O}_4^{L_H} = 0.085 p_V(I_4^{L_H})$. Then, in the particular case of $\theta = 45°$, the nonlocal fraction for $I_4^{L_S}$ is $p_V(I_4^{L_S}|45°) \approx 69.998 \%$ and $\mathcal{O}_4^{L_S} = 4.690 \%$ while $p_V(I_4^{L_H}|45°) \approx 10.627 \%$ and $\mathcal{O}_4^{L_H} \approx 0.953 \%$ (cf. Table I).

At this point, it is important to note that $p_V(I_4^{L_S}|45°)$ is significantly higher than the results previously achieved for Mermin-Ardehali-Belinskii-Klyshko and Werner-Wolf-Zukowski-Brukner inequalities, i.e., 10.002 % and 13.313 %, respectively [10,11]. Consequently, the problem of entanglement detection via random measurements discussed in Refs. [10,11] can be remarkably improved by matching the inequality class. Finally, it should be emphasized that $I_4^{L_S}$ ($I_4^{L_H}$) corresponds to 96 (1536) Bell expressions, which are equivalent under the relabeling of parties, inputs, and outputs. It means that all predictions described so far can be reconstructed (with precision up to $\mathcal{O}_4^{L_S}$ and $\mathcal{O}_4^{L_H}$) by considering just 96 instead of 53 856 Bell inequalities for the standard model and 1536 instead of 405 056 Bell inequalities for the hybrid model. In other words, it provides a great simplification

of the analyzed problems and thus facilitates experimental implementation.

Let us now discuss the structure of genuine nonlocal correlations more deeply. It is known that multipartite nonlocal correlations may have several origins [20–22], namely: the nonsignaling principle (NL_H set); time-order-dependent principle (T set), i.e., one-way signaling case; and Svetlichny principle (S_v set) where a two-way signaling scenario is assumed. For these sets the following relation is satisfied, $S_v \subset T \subset NL_H$, where the inclusion is strict [22].

The necessity to distinguish various kinds of genuine nonlocality comes from the perspective of classical simulations of quantum correlations in terms of shared random data and communication [36]. For instance, the model of T nonlocality is crucial for the simulation of quantum correlations in all protocols where measurements performed on a particular system may depend on the measurement outcome obtained from another system, e.g., measurement-based computation. For that reason, it is important to investigate the nonlocality of the subsets $NL_H|T$, $T|S_v$, and S_v. The first one denotes the nonlocal correlations which belong to the set NL_H but not to T and likewise for the later one. Obviously,

$$p_V(NL_H) = p_V(NL_H|T) + p_V(T)$$
$$= p_V(NL_H|T) + p_V(T|S_v) + p_V(S_v). \quad (8)$$

As we see in Table I and Fig. 2, the Svetlichny-type nonlocality is detected in extremely rare cases, with the probability below 0.55 %. This type of nonlocality is caused by violation of the Svetlichny inequality $I_{185}^{L_H}$ [20,22]. As the inequality $I_{185}^{L_H} \leqslant 1$ is satisfied when $\theta \leqslant 22.5°$ [30,37,38], the nonlocal fraction $p_V(S_v)$ also vanishes in this regime. In the case of $NL_H|T$ and $T|S_v$, the nonlocal fraction p_V is noticeably higher and reaches its maximal value of 6.3 % and 4.7 %, respectively. Interestingly, when $\theta \leqslant 22.5°$ the nonlocal fraction $p_V(T|S_v) > p_V(NL_H|T)$ (see Fig. 2), changing the origin of nonlocal correlations in this sense that the major impact to $p_V(NL_H)$, comes from the time-order-dependent model without nonsignaling principle assumption.

B. Nonlocal fraction in the presence of noise

Let us now verify whether the above-described observations are also satisfied when a more realistic scenario is taken into consideration. In any experimental preparation of the quantum state, various kinds of imperfections are inevitably present. They are caused, e.g., by improper setting of individual experimental components or by depolarization effects (presence of noise). As the influence of the first imperfection factor is rather hard to be expressed quantitatively, we concentrate on the later one. For that reason, we extend our calculations of the nonlocal fraction to the following state:

$$\rho = v|\theta\rangle\langle\theta| + \frac{1-v}{8}\mathbb{1}_8, \quad (9)$$

where $|\theta\rangle$ denotes pure gGHZ state, the parameter v is called the visibility of the state ($0 \leqslant v \leqslant 1$), and $\mathbb{1}_8$ stands for the identity matrix. In contemporary experiments, the gGHZ states were successfully generated with $v \approx 0.83$ [27–29] and recently even $v \approx 0.97$ [30].
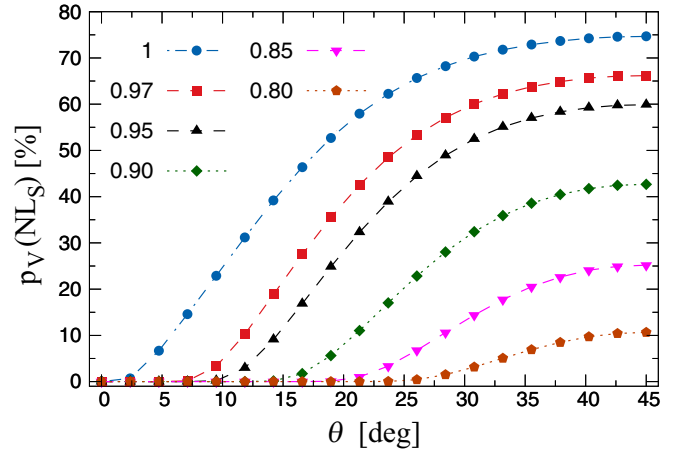

FIG. 3. Nonlocal fraction within standard local realism for gGHZ state. Presented curves refer to various $v \in (0.8, 1)$ as described in the legend.

It is known that the presence of noise implies a linear decline in the strength of violation. This is valid for both standard and hybrid models. Therefore, the ratio $\max(I^{L_S})/\max(I^{L_H})$, which describes the relation between the degree of standard and genuine tripartite nonlocality does not depend on v, as long as both inequalities are violated for a noisy state. In the case of p_V, the impact of noise is more complicated and stronger. First, it results in an exponential decay of p_V (see Figs. 3 and 4). This is clearly visible especially for the genuine nonlocality. For instance, if one takes the GHZ state and $v = 0.97$, as in the experiment discussed in Ref. [30], the nonlocal fraction $p_V(NL_H)$ decreases from 11.580% to 6.285%, i.e., becomes almost two times smaller with respect to the noiseless scenario. Furthermore, when $v < 0.90$ the nonlocal fraction $p_V(NL_H) < 0.7$ %. Consequently, all experiments performed with the visibility of the gGHZ state around 0.83 [27–29] yield $p_V(NL_H) < 0.05$ % and are, thus, hardly measurable. On the other hand, the nonlocal fraction $p_V(NL_S)$ for the GHZ state and $v = 0.97$ is equal
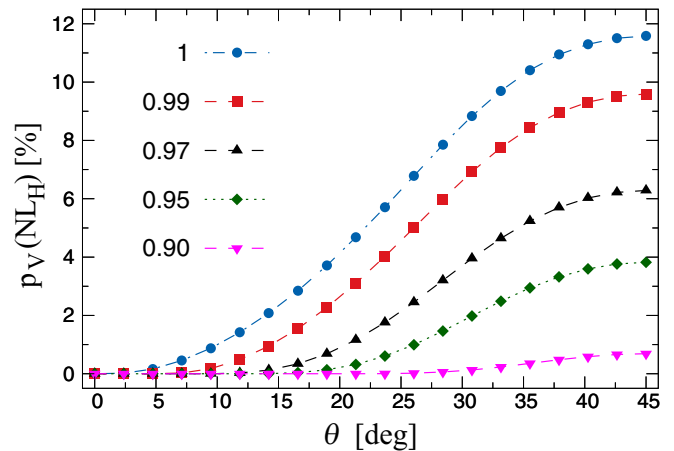

FIG. 4. Nonlocal fraction within hybrid local–nonlocal realism for gGHZ state. Presented curves refer to various $v \in (0.9, 1)$ as described in the legend.

to 66.117% (initially 74.688%). When v decreases to 0.85 then the nonlocal fraction $p_V(NL_S)$ drops down to 25.192%. It means that the presence of noise affects the results to varying degrees, depending on the chosen model of nonlocality. Therefore, the ratio $p_V(NL_S, v < 1)/p_V(NL_H, v < 1)$ becomes even greater than $p_V(NL_S, v = 1)/p_V(NL_H, v = 1)$ in the entire range of θ. For exact results see Appendix B: Tables IV and V.

Despite that, the dominant role of Bell inequalities $I_4^{L_S} \leqslant 1$ and $I_4^{L_H} \leqslant 1$ is also valid in the presence of noise (at least for $v \geqslant 0.8$). Therefore, we can generalize Eq. (7) in the following way:

$$p_V(NL_S, v) = p_V(I_4^{L_S}, v) + \mathcal{O}_4^{L_S}(v),$$

$$p_V(NL_H, v) = p_V(I_4^{L_H}, v) + \mathcal{O}_4^{L_H}(v), \tag{10}$$

where a potential approximation of both error functions [linear with respect to $p_V(I_4^{L_S}, v)$] are given by $\mathcal{O}_4^{L_S}(v) = (4.074 - 7.611v + 3.607v^2) p_V(I_4^{L_S}, v)$ and $\mathcal{O}_4^{L_H}(v) = [0.002559/(v^3 - 2.91497v^2 + 2.833967v - 0.916638) - 1] p_V(I_4^{L_H}, v)$.

C. Nonlocal fraction versus tripartite entanglement

We stress that in all cases analyzed above, the nonlocal fraction p_V increases with θ. Similar behavior is expected for the tripartite entanglement of the gGHZ state. For that reason, it is important to compare these two quantities.

It is known that when the gGHZ state is mixed with white noise, its entanglement properties change with the v parameter. Depending on the visibility, the resulting state ρ belongs to different entanglement classes, defined as inequivalent under stochastic local operations and classical communication [39]. As the genuine tripartite nonlocality occurs in both the GHZ and W class [40], the appropriate tripartite entanglement measure is the genuine concurrence C_{GME} which vanishes only for biseparable and fully separable states [41]. For the noisy-gGHZ state, ρ, the genuine concurrence is given by $C_{GME}(\rho) = \max\{0, v\sin(2\theta) - \frac{2(1-v)}{3}\}$. As we see, for constant v the genuine concurrence $C_{GME}(\rho)$ always increases with θ. For instance, when $v = 1$ then the genuine concurrence behaves as $C_{GME}(|\theta\rangle) = \sin(2\theta)$. Consequently, one can expect that p_V is a monotonic function of tripartite entanglement and vice versa.

The lack of analytical expression for p_V prohibits us from writing an exact relation between tripartite entanglement and nonlocal fraction. However, we can still find its approximation. In particular, for the genuine nonlocality such an outcome looks very interesting. Specifically, using nonlinear regression one can obtain a simple formula

$$C_{GME}^2(\rho) = \alpha_0\, p_V(NL_H, v) + \alpha_1 \sqrt{p_V(NL_H, v)}$$
$$+ 3.7(1 - v), \tag{11}$$

where $\alpha_0 = 14.79\,[1.0064\sin(0.511 + v) - 1]$ and $\alpha_1 = -13.14 + 32.51v - 19.31v^2$. As we see, none of the coefficients α_0 and α_1 depend on the angle θ. Such a dependence is hidden within $p_V(NL_H, v)$ as given in Table I and Appendix B. The last term in Eq. (11) is caused by the fact that entanglement and nonlocality have different critical visibility, i.e., there exist tripartite entangled states which are
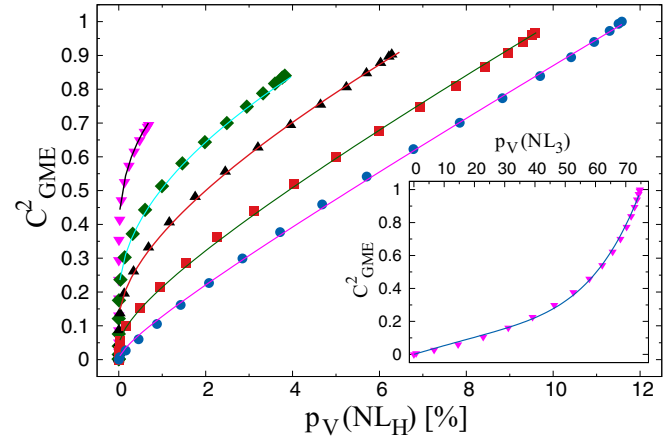

FIG. 5. Relation between genuine concurrence C_{GME}^2 and nonlocal fraction $p_V(NL_H)$. Presented symbols correspond to numerical outcomes, where $p_V(NL_H) \equiv p_V^{NL_H}(|\theta\rangle, v)$ are given in Table I and Appendix B, and $C_{GME}(\rho) = \max\{0, v\sin(2\theta) - \frac{2(1-v)}{3}\}$. The shape of symbols denotes: $v = 1$ (circuit symbols), $v = 0.99$ (square symbols), $v = 0.97$ (triangle symbols), $v = 0.95$ (diamond symbols), and $v = 0.90$ (reversed triangle symbols). Solid lines correspond to Eq. (11) with various v. The inset shows C_{GME}^2 as a function of $p_V(NL_S)$ for $v = 1$. The corresponding fitting function is given by $C_{GME}^2(|\theta\rangle) = 0.00542\,p_V(NL_S) - 1.47 \times 10^{-5} p_V(NL_S)^2 + 2.8386 \times 10^{-10} p_V(NL_S)^5$.

not genuine tripartite nonlocal (see, for instance, Ref. [40]). As we see in Fig. 5, the quality of our approximation of C_{GME}^2 is very good. In particular, when visibility $v = 1$ Eq. (11) reduces to

$$C_{GME}^2(|\theta\rangle) = 0.068\, p_V(NL_H) + 0.06\sqrt{p_V(NL_H)}, \tag{12}$$

and such an approximation provides the coefficient of determination $R^2 = 0.999$. It means that by measuring the nonlocal fraction $p_V(NL_H)$ one can directly estimate the genuine concurrence $C_{GME}^2(|\theta\rangle)$ with precision ± 0.012. In the general case, the estimation precision of genuine concurrence by Eq. (11) is not greater than ± 0.016. Moreover, using Eq. (7) the above relation can be further modified to reduce the number of analyzed Bell inequalities, as mentioned before.

By analogy, one can perform a numerical approximation of $C_{GME}^2(\rho)$ with respect to other sets of nonlocality [$p_V(NL_S)$, $p_V(NL_H|T)$ etc.]. However, in all such cases, the fitting function takes much more complicated form. For instance, $C_{GME}^2(|\theta\rangle)$ vs $p_V(NL_S)$ require the polynomial approximation of fifth order (see inset in Fig. 5). Furthermore, in general, the nonzero value of $p_V(NL_S)$ does not guarantee $C_{GME}^2(|\theta\rangle) \neq 0$ as mentioned in Ref. [14].

D. Nonlocal fraction of individual Bell inequalities

Despite the utility of inequalities $I_4^{L_S}$ and $I_4^{L_H}$ described above, in general the conclusions resulting from a given Bell inequality may be inconsistent with the behavior of the whole set of nonlocal correlations. For instance, the monotonic relation between nonlocal fraction p_V and tripartite entanglement is not always satisfied if one assumes *a priori* fixed Bell inequality. To highlight this fact, this paragraph is dedicated to the description of several examples of Bell inequalities
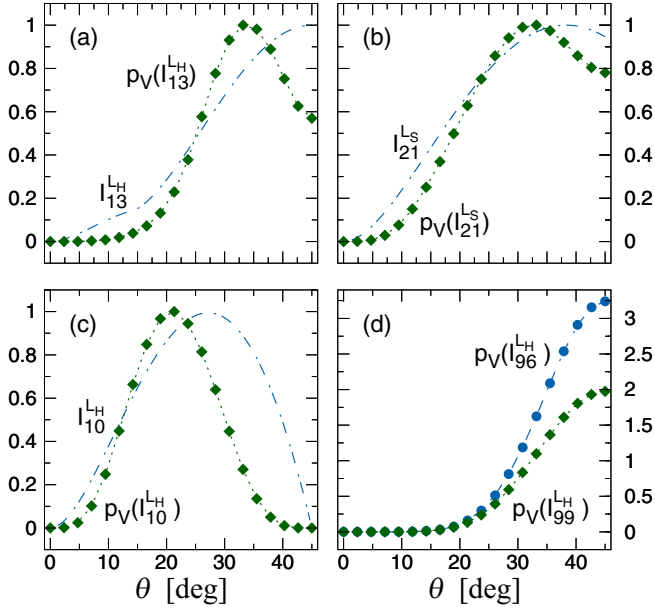
FIG. 6. Comparison between nonlocal fraction p_V and the strength of violation for various Bell inequalities.

which, applied to the gGHZ states, demonstrate various kinds of anomalies.

Let us start with the 13th facet inequality of the L_H polytop [22]. Then, for the gGHZ states both the tripartite entanglement and the strength violation of $I_{13}^{L_H} \leqslant 1$ increase monotonically with θ. Despite that the nonlocal fraction $p_V(I_{13}^{L_H})$ reaches its maximum for $\theta \approx 33°$ [see Fig. 6(a)]. In other words, we have an anomaly between C_{GME} and p_V, which is an analogy of the original anomaly reported in Refs. [9,42,43].

On the other hand, if one takes the 21st facet inequality of L_S or the 10th facet inequality of L_H (examined in Ref. [30]), then two kinds of anomalies are observed, namely, the anomaly between entanglement and nonlocality and the anomaly between the strength of violation and the nonlocal fraction [Figs. 6(b) and 6(c)]. Specifically, based on the calculations presented in Ref. [30] one can find that max $[I_{10}^{L_H}(\theta)]$ occurs when $\theta = 27°$ while the maximum of $p_V(I_{10}^{L_H})$ is located around $\theta = 21°$.

A similar situation was described in Ref. [15] in the context of Collins-Gisin-Linden-Masser-Popescu inequality [44]. It was shown that the anomaly between entanglement and nonlocality occurs regardless of the method used to measure nonlocality, despite the nonlocal fraction for the entire polytope increases monotonically with entanglement [16].

All these examples confirm that the behavior of p_V for individual Bell inequality may be significantly different than results presented in previous sections.

Finally, it is worth mentioning that even if two Bell inequalities are violated with the same strength, the nonlocal fraction does not have to be the same. As an example let us take the 96th and 99th facet inequalities of L_H. It was shown that max $[I_{96}^{L_H}(\theta)] \equiv$ max $[I_{99}^{L_H}(\theta)]$ in the entire range of θ [30]. However, $p_V(I_{96}^{L_H}) > p_V(I_{99}^{L_H})$ as presented in Fig. 6(d). Although such behavior is not surprising, it still deserves confirmation.
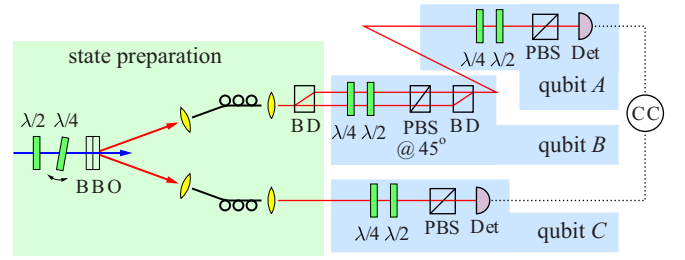

FIG. 7. Scheme of the experimental setup, in the state preparation part on the left three-qubit gGHZ states are generated, on the right three preparation parts are drown. $\lambda/2$: half-wave plate; $\lambda/4$: quarter-wave plate; BBO: double crystal cascade; PC: polarization controller; BD: beam displacer; PBS: polarizing beam splitter; Det: detector.

E. Experimental verification

To verify the above-described theoretical predictions, we perform experiments generating and measuring the nonlocal fraction on three-qubit generalized GHZ states of the form (6). Our experimental setup is depicted in Fig. 7. First, we generate polarization-entangled pairs of photons in the process of Type-I spontaneous parametric down-conversion. To achieve that, a laser beam of about 200mW pumps a cascade of two β-BaB$_2$O$_4$ (BBO) crystals [45–47]. These crystals have their optical axes rotated to mutually orthogonal planes, and because of the coherence of the pumping beam, the cascade generates an indistinguishable superposition of horizontally and vertically polarized photon pairs. Note that the probability of generating two pairs simultaneously is negligible. Labeling horizontal (vertical) polarization $|0\rangle$ ($|1\rangle$), the state generated immediately behind the crystal cascade reads

$$\cos\theta|00\rangle + \sin\theta|11\rangle, \qquad (13)$$

having the parameter θ set by controlling the pumping beam polarization.

Once generated, one photon of the pair is brought to a beam displacer (BD), where we encode an additional qubit into its spatial mode. If horizontally ($|0\rangle$) polarized, this photon maintains its spatial mode (associated with logical state $|0\rangle$), but when vertically ($|1\rangle$) polarized, the photon's spatial mode changes to spatial mode that we associate with logical state $|1\rangle$). The second photon does not undergo such an operation. As a result, we obtain a generalized three-qubit GHZ state in the form of

$$|\theta\rangle = \cos\theta|000\rangle_{ABC} + \sin\theta|111\rangle_{ABC} \qquad (14)$$

with the first qubit (A) corresponding to the spatially encoded qubit of the first photon. The second (B) and third (C) qubits correspond to polarization-encoded qubits of the first and second photons, respectively.

To implement local measurements on polarization-encoded qubits B and C, we subject the photons to standard polarization projections consisting of quarter- and half-wave plates followed by polarizers. The measurement on the spatially encoded qubit A is achieved afterwards by having the first photon spatial modes (already polarization-projected) interact on another beam displaced converting the spatial encoding to polarization encoding. Then a standard polarization projection

is used to measure the state of qubit A. The freedom in choosing local measurement bases allows us to subject the three qubits to all combinations of local projections onto $|0\rangle, |1\rangle, \frac{1}{\sqrt{2}}(|0\rangle \pm |1\rangle), \frac{1}{\sqrt{2}}(|0\rangle \pm i|1\rangle)$ states corresponding to a complete tomography of the three-qubit state [47] from which its density matrix can be estimated. We were able to adjust the parameter $\theta = 45°$ with a precision of $\pm 0.5°$. We observed the typical value of fidelity of the generated state to be 0.973 ± 0.009, i.e., the estimated visibility $v = 0.97 \pm 0.01$ (for details see Ref. [30]).

To measure any correlation coefficient, we set accordingly the six wave plates in the three projection parts of the setup and measure coincidence counts on the two detectors, denoted N_{xyz}^{abc}. This quantity is proportional to the probability that Alice, Bob, and Charlie observe outcomes a, b, c when measuring in bases x, y, z [see projectors (2)]. The proportion constant is the overall state generation rate. To link the experimental results with the above-described theory we have to properly normalize measured coincidences. That is why we measure also all seven orthogonal projections. As a result, the expectation value in the x, y, z setting reads

$$\langle A_x B_y C_z \rangle = \frac{\sum_{abc \in \{0,1\}} (-1)^{a+b+c} N_{xyz}^{abc}}{\sum_{abc \in \{0,1\}} N_{xyz}^{abc}}, \tag{15}$$

and similarly for other correlation coefficients: $\langle A_x \rangle$, $\langle A_x B_y \rangle$, and so on (see, for instance, Ref. [30]). Using correlation coefficients, the violation of individual Bell inequalities $I^{L_S} \leqslant 1$ and $I^{L_H} \leqslant 1$ is verified. As an example, let us consider the 4th facet inequality $I_4^{L_S} \leqslant 1$, where $I_4^{L_S} = [\langle A_0 B_0 \rangle + \langle A_0 B_0 C_1 \rangle - \langle A_0 B_1 \rangle - \langle A_0 B_1 C_1 \rangle + \langle A_1 B_0 \rangle + \langle A_1 B_0 C_1 \rangle + \langle A_1 B_1 \rangle + \langle A_1 B_1 C_1 \rangle - 2\langle C_1 \rangle]/2$. Then, for the particular set of angles

$$\begin{aligned}
\phi_0^A &= 45°, & \chi_0^A &= -120°, \\
\phi_1^A &= 71°, & \chi_1^A &= -120°, \\
\phi_0^B &= 60°, & \chi_0^B &= 60°, \\
\phi_1^B &= 60°, & \chi_1^B &= 240°, \\
\phi_0^C &= 60°, & \chi_0^C &= 60°, \\
\phi_1^C &= 60°, & \chi_1^C &= 240°,
\end{aligned} \tag{16}$$

and all $\gamma_i^j = 0$, we found the experimental value

$$I_4^{L_S} = 1.1286 \pm 0.015, \tag{17}$$

which is in line with theoretical prediction $I_4^{L_S} = 1.114$.

However, such experimental results received from measured coincidence rates, in principal, fluctuate due to shot noise. It means that Bell expressions I which, for the GHZ state, give the outcomes close to the upper threshold are unsuitable for experimental verification of the nonlocal fraction since a violation of the inequality $I \leqslant 1$ might be simply accidental (due to shot noise). As an example of such Bell expression see $I_{10}^{L_H}$ discussed in Section D (see for instance Fig. 6(c)) and Ref. [30]. That is why we selected the more robust calculation based on the 4th facet inequalities, $I_4^{L_S} \leqslant 1$ and $I_4^{L_H} \leqslant 1$. To determine the nonlocal fraction both inequalities have been tested for 10^5 randomly chosen settings. As a

result we found that

$$p_V(I_4^{L_S}, v) = 56\% \pm 5\%,$$

$$p_V(I_4^{L_H}, v) = 6\% \pm 2\%. \tag{18}$$

Theoretical values for these quantities are $p_V(I_4^{L_S}, v = 0.97) = 61.144\%$ and $p_V(I_4^{L_H}, v = 0.97) = 5.672\%$ (see Appendix B: Tables II and III). As we see, our measurements are in complete agreement with theoretical predictions.

The error bars of p_V were estimated by properly shifting the upper threshold of Bell inequalities $I_4^{L_S}$ and $I_4^{L_H}$. Specifically, our experimental determination of $I_4^{L_S}$ and $I_4^{L_H}$ are performed with uncertainties not greater than 0.015. It means that for all settings which provide $|I^{L_S} - 1| \leqslant 0.015$ ($|I^{L_H} - 1| \leqslant 0.015$) one cannot unambiguously verify whether Bell inequality $I^{L_S} \leqslant 1$ ($I^{L_H} \leqslant 1$) is violated or not. Following the propagation of the uncertainty theorem, we calculate p_V for two boundary cases: (i) assuming that $I^{L_S} > 0.985$ ($I^{L_H} > 0.985$) is nonlocal, and (ii) assuming that $I^{L_S} \leqslant 1.015$ ($I^{L_H} \leqslant 1.015$) is local. In this way the error bars of p_V were estimated.

IV. CONCLUSION

In this paper we investigated the nonlocal fraction as an indicator of nonlocal correlations. While such as analysis was successfully used in many recent papers, several crucial aspect were not addressed. The main limitation of these studies is that the standard local realistic model is used to witness nonlocal correlations in multipartite state. In our work, we provided alternative calculations for the genuine multipartite nonlocality.

We applied that idea to the tripartite GHZ state and showed that the probability of finding a genuine nonlocal correlation is significantly smaller than for the standard nonlocality. Interestingly, it is even smaller than results previously obtained for the bipartite GHZ counterpart. While the nonlocal fraction for standard realistic model rapidly tends to unity as the number of parties increases, it is unknown whether such behavior is valid for hybrid local–nonlocal realistic models. Our result for the tripartite state indicates a rather opposite scenario and provides a motivation for further work. Naturally, this result could be an anomaly and for n-partite GHZ states ($n > 3$) the nonlocal fraction should tend to unity. However, we see no argument to expect that. In a more general context, our result suggests a negative answer to the question whether without a shared reference frame, a violation of a genuine n-partite Bell inequality can still be demonstrated reliably without resorting to complicated state preparation or the consumption of expensive quantum resources, which is in contradiction with standard nonlocality [10].

Furthermore, we clearly showed that the tripartite genuine concurrence is a monotonic function of the nonlocal fraction. An increase of the later implies growth of entanglement, which solves the anomaly observed between entanglement and nonlocality when using other measures. Moreover, we proposed the formula which allows for experimental estimation of genuine concurrence C_{GME} by using $p_V(L_H)$.

For real-world applications of our results, we investigated their robustness against decoherence. We showed that the

influence of noise affects the results to varying degrees, depending on the chosen model of nonlocality. The strongest impact was observed for genuine nonlocality, showing that an experimental detection of $p_V(L_H)$ requires the use of generalized GHZ state with visibility $v > 0.9$. Otherwise, the nonlocal fraction $p_V(L_H) < 0.07\,\%$.

Finally, we studied the statistical relevance of various classes of tight Bell inequalities showing a dominant role of two of them. Using these two classes one can estimate the nonlocal fraction for both standard and hybrid realistic model. Such an estimation was also investigated experimentally, showing a good agreement with theoretical predictions.

APPENDIX A

The 2nd or 15th facet Bell inequality for standard realistic model are given by

$$
\begin{aligned}
I_2^{Ls} &= \tfrac{1}{2}(\langle A_0 B_0 C_0\rangle + \langle A_1 B_1 C_0\rangle + \langle A_1 B_0 C_1\rangle - \langle A_0 B_1 C_1\rangle) \leqslant 1, \\
I_{15}^{Ls} &= \tfrac{1}{4}(2\langle A_0 B_0\rangle + 2\langle A_1 B_0\rangle + \langle A_0 C_0\rangle + \langle A_1 C_0\rangle - 2\langle B_0 C_0\rangle \\
&\quad + \langle A_0 C_1\rangle + \langle A_1 C_1\rangle - 2\langle B_0 C_1\rangle \\
&\quad + \langle A_0 B_1 C_0\rangle - \langle A_0 B_1 C_1\rangle - \langle A_1 B_1 C_0\rangle + \langle A_1 B_1 C_1\rangle) \leqslant 1,
\end{aligned}
$$
(A1)

where we assume to have an ensemble of projective measurement $A_0 = \vec{a}_0 \cdot \vec{\sigma}_A$, or $A_1 = \vec{a}_1 \cdot \vec{\sigma}_A$ on qubit A, $B_0 = \vec{b}_0 \cdot \vec{\sigma}_B$, or $B_1 = \vec{b}_1 \cdot \vec{\sigma}_B$ on qubit B, $C_0 = \vec{c}_0 \cdot \vec{\sigma}_C$, or $C_1 = \vec{c}_1 \cdot \vec{\sigma}_C$ on qubit C. The vector $\vec{\sigma} = \{\sigma_x, \sigma_y, \sigma_z\}$, where σ_x, σ_y, and σ_z denote the Pauli operators associated with three orthogonal directions.

To find a global maximum of $\hat{I}_2^{Ls}$ and $\hat{I}_{15}^{Ls}$ for the gGHZ state a similar method as in Refs. [30,40] was applied. First, we represent all unit vectors in spherical coordinates, i.e., $\vec{a}_0 = (\sin 2\phi_0^a \cos \xi_0^a, \sin 2\phi_0^a \sin \xi_0^a, \cos 2\phi_0^a)$ and likewise for similarly defined terms. The notation is chosen in such a way to be in line with Eq. (3). Our aim is to find a set of optimal spherical angles for all measurements $A_0,...,C_1$. Without lose of generality, we restrict our calculation to azimuthal angles in the interval $[0, \pi/2]$ and polar angles in $[0, 2\pi]$.

Let us now concentrate at $\hat{I}_{15}^{Ls}$. First, we rewrite $\hat{I}_{15}^{Ls}$ in terms of unit vectors $\vec{d}_0$ and $\vec{d}_1$ defined such that $\vec{c}_0 + \vec{c}_1 = 2\vec{d}_0 \cos \eta$ and $\vec{c}_0 - \vec{c}_1 = 2\vec{d}_1 \sin \eta$. Note that

$$
\vec{d}_0 \cdot \vec{d}_1 = \cos \theta_0^d \cos \theta_1^d + \sin \theta_0^d \sin \theta_1^d \cos(\phi_0^d - \phi_1^d) = 0.
$$
(A2)

Then, with settings $D_0 = \vec{d}_0 \cdot \vec{\sigma}_C$ and $D_1 = \vec{d}_1 \cdot \vec{\sigma}_C$ one obtains

$$
\begin{aligned}
I_{15}^{Ls} &= \tfrac{1}{2}(\langle A_0 B_0\rangle + \langle A_1 B_0\rangle + \langle (A_0 + A_1 - 2B_0) D_0\rangle \cos \eta \\
&\quad + \langle (A_0 - A_1) B_1 D_1\rangle \sin \eta).
\end{aligned}
$$
(A3)

Now, for the gGHZ state

$$
\frac{\partial I_{15}^{Ls}}{\partial \phi_0^d} = -2(\cos 2\phi_0^a + \cos 2\phi_1^a - 2\cos 2\phi_0^b)\cos 2\phi_0^d, \quad (A4)
$$

and the global maximum is reached when $\partial I_{15}^{Ls}/\partial \phi_0^d = 0$, i.e., when $\phi_0^d = 0, \pi/2$. Substituting this result into Eq. (A2) yields $\phi_1^d = \pi/4$. Consequently, when inserting $\{\phi_0^d, \phi_1^d\} =$

TABLE II. Nonlocal fraction, $p_V(I_4^{Ls}, v)$, for Bell inequality I_4^{Ls} and generalized GHZ state $\rho = v|\theta\rangle\langle\theta| + \frac{1-v}{8}\mathbb{1}_8$.

θ	$v = 1.0$	$v = 0.99$	$v = 0.97$	$v = 0.95$	$v = 0.90$	$v = 0.85$	$v = 0.80$	$v = 0.75$	$v = 0.70$
45.	69.998	67.173	61.144	54.731	37.671	21.07	7.976	1.08	0.002
42.632	69.928	67.088	61.047	54.604	37.485	20.865	7.796	1.005	0.0
40.263	69.614	66.76	60.658	54.136	36.833	20.155	7.26	0.817	0.0
37.895	69.046	66.133	59.909	53.261	35.657	18.888	6.324	0.543	0.0
35.526	68.23	65.226	58.808	51.958	33.928	17.091	5.085	0.266	0.0
33.158	67.102	63.977	57.266	50.112	31.5	14.745	3.673	0.067	0.0
30.789	65.633	62.297	55.201	47.649	28.363	11.913	2.22	0.002	0.0
28.421	63.694	60.088	52.425	44.376	24.48	8.76	1.006	0.0	0.0
26.053	61.3	57.319	48.967	40.321	19.932	5.584	0.232	0.0	0.0
23.684	58.224	53.785	44.579	35.338	14.888	2.771	0.006	0.0	0.0
21.316	54.443	49.437	39.28	29.441	9.68	0.808	0.0	0.0	0.0
18.947	49.806	44.113	32.949	22.709	4.928	0.052	0.0	0.0	0.0
16.579	44.182	37.725	25.633	15.428	1.488	0.0	0.0	0.0	0.0
14.21	37.634	30.317	17.6	8.31	0.095	0.0	0.0	0.0	0.0
11.842	30.208	22.024	9.576	2.667	0.0	0.0	0.0	0.0	0.0
9.474	22.361	13.45	3.049	0.166	0.0	0.0	0.0	0.0	0.0
7.105	14.383	5.571	0.131	0.0	0.0	0.0	0.0	0.0	0.0
4.737	6.607	0.534	0.0	0.0	0.0	0.0	0.0	0.0	0.0
2.368	0.725	0.0	0.0	0.0	0.0	0.0	0.0	0.0	0.0
0.0	0.0	0.0	0.0	0.0	0.0	0.0	0.0	0.0	0.0

TABLE III. Nonlocal fraction, $p_V(I_4^{L_H}, v)$, for Bell inequality $I_4^{L_H}$ and generalized GHZ state $\rho = v|\theta\rangle\langle\theta| + \frac{1-v}{8}\mathbb{1}_8$.

θ	$v = 1.00$	$v = 0.99$	$v = 0.97$	$v = 0.95$	$v = 0.90$	$v = 0.85$	$v = 0.80$
45.00	10.627	8.773	5.672	3.363	0.489	0.006	0.0
42.63	10.569	8.712	5.615	3.313	0.472	0.006	0.0
40.26	10.372	8.513	5.43	3.161	0.425	0.004	0.0
37.89	10.023	8.167	5.119	2.911	0.352	0.002	0.0
35.53	9.487	7.649	4.671	2.568	0.266	0.001	0.0
33.16	8.762	6.962	4.104	2.157	0.18	0.00023	0.0
30.79	7.856	6.125	3.453	1.714	0.105	0.000022	0.0
28.42	6.816	5.187	2.758	1.266	0.049	0.0	0.0
26.05	5.692	4.200	2.07	0.856	0.016	0.0	0.0
23.68	4.559	3.229	1.438	0.512	0.003	0.0	0.0
21.32	3.482	2.335	0.904	0.259	0.0001	0.0	0.0
18.95	2.497	1.554	0.491	0.1	0.0	0.0	0.0
16.58	1.666	0.93	0.216	0.024	0.0	0.0	0.0
14.21	1.007	0.478	0.066	0.002	0.0	0.0	0.0
11.84	0.535	0.195	0.010	0.0	0.0	0.0	0.0
9.47	0.237	0.053	0.0002	0.0	0.0	0.0	0.0
7.11	0.082	0.007	0.0	0.0	0.0	0.0	0.0
4.74	0.020	0.00001	0.0	0.0	0.0	0.0	0.0
2.37	0.002	0.0	0.0	0.0	0.0	0.0	0.0

$\{0, \pi/4\}$ into Eq. (A3) one has

$$
\begin{aligned}
I_{15}^{L_S} = \tfrac{1}{2}\big[& 2\cos\left(\phi_0^a - \phi_1^a\right)\cos\left(\phi_0^a + \phi_1^a\right)\cos 2\phi_0^b \\
& + \left(\cos 2\phi_0^a + \cos 2\phi_1^a - 2\cos 2\phi_0^b\right)\cos\eta \\
& + \sin 2\theta \sin 2\phi_1^b\big(\sin 2\phi_0^a \cos\xi_0^{abd} \\
& - \sin 2\phi_1^a \cos\xi_1^{abd}\big)\sin\eta\big],
\end{aligned} \tag{A5}
$$

where $\xi_0^{abd} = \xi_0^a + \xi_1^b + \xi_1^d$ and $\xi_1^{abd} = \xi_1^a + \xi_1^b + \xi_1^d$. From Eq. (A5) it is easy to notice that the maximum is obtained for $\phi_1^b = \pi/4$ and then, $\partial I_{15}^{L_S}/\partial\phi_0^b = 0$ when $\phi_0^b = \pi/2$. Furthermore, if one solves $\partial I_{15}^{L_S}/\partial\xi_0^{abd} = \partial I_{15}^{L_S}/\partial\xi_1^{abd} = 0$ then

$\xi_0^{abd} = \pi$ and $\xi_1^{abd} = 0$. As a result we have

$$
\begin{aligned}
I_{15}^{L_S} = \tfrac{1}{2}\big[& -2\cos\left(\phi_0^a - \phi_1^a\right)\cos\left(\phi_0^d + \phi_1^d\right) \\
& + \left(\cos 2\phi_0^a + \cos 2\phi_1^a + 2\right)\cos\eta \\
& - \sin 2\theta\left(\sin 2\phi_0^a + \sin 2\phi_1^a\right)\sin\eta\big].
\end{aligned} \tag{A6}
$$

Now, solving $\partial I_{15}^{L_S}/\partial\phi_0^a = \partial I_{15}^{L_S}/\partial\phi_1^a = 0$ we obtain $\phi_0^a = \phi_1^a$.

TABLE IV. Nonlocal fraction within standard local realism, $p_V(L_S, v)$, for generalized GHZ state $\rho = v|\theta\rangle\langle\theta| + \frac{1-v}{8}\mathbb{1}_8$.

θ	$v = 0.99$	$v = 0.97$	$v = 0.95$	$v = 0.90$	$v = 0.85$	$v = 0.80$	$v = 0.75$	$v = 0.70$	$v = 0.65$	$v = 0.62$	$v = 0.60$
45.00	74.059	68.117	61.59	43.485	25.192	10.332	2.186	0.458	0.147	0.057	0.026
42.63	73.652	67.708	61.166	43.106	24.877	10.088	2.071	0.43	0.134	0.051	0.023
40.26	72.986	66.977	60.373	42.195	23.949	9.367	1.765	0.377	0.113	0.043	0.019
37.89	72.021	65.889	59.171	40.709	22.388	8.158	1.313	0.29	0.079	0.027	0.011
35.53	70.811	64.477	57.554	38.645	20.223	6.584	0.841	0.199	0.047	0.013	0.004
33.16	69.286	62.644	55.377	35.813	17.407	4.773	0.433	0.113	0.021	0.005	0.001
30.79	67.366	60.289	52.585	32.201	14.02	2.916	0.195	0.049	0.006	0.001	0.0
28.42	64.873	57.171	48.901	27.735	10.25	1.351	0.077	0.014	0.001	0.0	0.0
26.05	61.77	53.297	44.343	22.506	6.455	0.344	0.019	0.002	0.0	0.0	0.0
23.68	57.796	48.393	38.744	16.695	3.12	0.024	0.001	0.0	0.0	0.0	0.0
21.32	52.891	42.44	32.124	10.723	0.874	0.0	0.0	0.0	0.0	0.0	0.0
18.95	46.902	35.38	24.617	5.372	0.055	0.0	0.0	0.0	0.0	0.0	0.0
16.58	39.81	27.356	16.632	1.576	0.0	0.0	0.0	0.0	0.0	0.0	0.0
14.21	31.769	18.693	8.9	0.097	0.0	0.0	0.0	0.0	0.0	0.0	0.0
11.84	22.912	10.111	2.812	0.0	0.0	0.0	0.0	0.0	0.0	0.0	0.0
9.47	13.906	3.188	0.168	0.0	0.0	0.0	0.0	0.0	0.0	0.0	0.0
7.11	5.723	0.132	0.0	0.0	0.0	0.0	0.0	0.0	0.0	0.0	0.0
4.74	0.543	0.0	0.0	0.0	0.0	0.0	0.0	0.0	0.0	0.0	0.0
2.37	0.0	0.0	0.0	0.0	0.0	0.0	0.0	0.0	0.0	0.0	0.0

TABLE V. Nonlocal fraction within hybrid local–nonlocal realism, $p_V(L_H, v)$, for generalized GHZ state $\rho = v|\theta\rangle\langle\theta| + \frac{1-v}{8}\mathbb{1}_8$.

θ	$v = 0.99$	$v = 0.97$	$v = 0.95$	$v = 0.90$	$v = 0.85$	$v = 0.80$	$v = 0.75$	$v = 0.72$
45.00	9.590	6.285	3.821	0.686	0.052	0.004	0.0001	0.0
42.63	9.520	6.218	3.765	0.660	0.047	0.004	0.00008	0.0
40.26	9.312	6.026	3.597	0.587	0.037	0.002	0.00003	0.0
37.89	8.960	5.702	3.322	0.480	0.023	0.001	0.000001	0.0
35.53	8.441	5.238	2.945	0.355	0.011	0.0002	0.0	0.0
33.16	7.754	4.644	2.489	0.233	0.004	0.00001	0.0	0.0
30.79	6.926	3.953	1.980	0.130	0.0007	0.0	0.0	0.0
28.42	5.993	3.202	1.463	0.060	0.00007	0.0	0.0	0.0
26.05	5.002	2.451	0.993	0.021	0.000002	0.0	0.0	0.0
23.68	4.024	1.757	0.605	0.004	0.0	0.0	0.0	0.0
21.32	3.107	1.161	0.320	0.0003	0.0	0.0	0.0	0.0
18.95	2.270	0.683	0.135	0.000003	0.0	0.0	0.0	0.0
16.58	1.545	0.340	0.038	0.0	0.0	0.0	0.0	0.0
14.21	0.947	0.125	0.004	0.0	0.0	0.0	0.0	0.0
11.84	0.485	0.024	0.00002	0.0	0.0	0.0	0.0	0.0
9.47	0.174	0.0007	0.0	0.0	0.0	0.0	0.0	0.0
7.11	0.025	0.0	0.0	0.0	0.0	0.0	0.0	0.0
4.74	0.00007	0.0	0.0	0.0	0.0	0.0	0.0	0.0
2.37	0.0	0.0	0.0	0.0	0.0	0.0	0.0	0.0

Then, after some standard algebra the global maximum of Eq. (A6) is reached when $\phi_0^a = \arctan(-\sqrt{\frac{1+\cos\theta\sin\theta}{\cos\theta\sin\theta}})$ and $\eta = 2\arctan(\sqrt{\frac{1}{1+\cos\theta\sin\theta}})$. Consequently

$$I_{15}^{L_S} \leqslant \frac{\sin(2\theta)[1+\sin(2\theta)]+1}{1+\sin(2\theta)}. \tag{A7}$$

The set of measurement angles that provides the equality in the above expression is given by

$$\theta_{a1} = \theta_{a2} = 2\arctan(\sqrt{1+\cot\theta+\tan\theta});$$
$$\theta_{b1} = \pi; \theta_{b2} = \frac{3\pi}{2};$$

$$\theta_{c1} = \theta_{c2} = 2\arctan(1/\sqrt{1+\cot\theta+\tan\theta}),$$
$$\phi_{a1} = \phi_{b1} = \phi_{c1} = 0; \phi_{a2} = \phi_{c2} = \pi; \phi_{b2} = 3\pi. \tag{A8}$$

In the same way one can get

$$I_2^{L_S} \leqslant 2\sin(2\theta), \tag{A9}$$

which is saturated for the following set of unit vectors:

$$\theta_{a1} = \theta_{b1} = \theta_{c1} = \frac{\pi}{2}; \theta_{a2} = \theta_{b2} = \theta_{c2} = \frac{3\pi}{2},$$
$$\phi_{a1} = \phi_{b1} = \phi_{c1} = 0; \phi_{a2} = -\phi_{b2} = -\phi_{c2} = \frac{\pi}{2}. \tag{A10}$$

APPENDIX B

In Tables III–V we provide a complete results of nonlocal fraction for various indicators of nonlocality.

[1] J. S. Bell, Physics **1**, 195 (1964).

[2] N. Brunner, D. Cavalcanti, S. Pironio, V. Scarani, and S. Wehner, Rev. Mod. Phys. **86**, 419 (2014).

[3] A. K. Ekert, Phys. Rev. Lett. **67**, 661 (1991).

[4] J. Barrett, L. Hardy, and A. A. Kent, Phys. Rev. Lett. **95**, 010503 (2005).

[5] A. Acín, N. Brunner, N. Gisin, S. Massar, S. Pironio, and V. Scarani, Phys. Rev. Lett. **98**, 230501 (2007).

[6] S. Pironio *et al.*, Nature **464**, 1021 (2010).

[7] A. A. Méthot and V. Scarani, Quant. Inf. Comput. **7**, 157 (2007).

[8] S. D. Bartlett, T. Rudolph, and R. W. Spekkens, Rev. Mod. Phys. **79**, 555 (2007).

[9] A. Acín, T. Durt, N. Gisin, and J. I. Latorre, Phys. Rev. A **65**, 052325 (2002).

[10] Y.-C. Liang, N. Harrigan, S. D. Bartlett, and T. Rudolph, Phys. Rev. Lett. **104**, 050401 (2010).

[11] J. J. Wallman, Y.-C. Liang, and S. D. Bartlett, Phys. Rev. A **83**, 022110 (2011).

[12] V. Lipinska, F. Curchod, A. Máttar, and A. Acín, New J. Phys. **20**, 063043 (2018).

[13] E. A. Fonseca and F. Parisio, Phys. Rev. A **92**, 030101(R) (2015).

[14] A. de Rosier, J. Gruca, F. Parisio, T. Vértesi, and W. Laskowski, Phys. Rev. A **96**, 012101 (2017).

[15] A. Barasiński and M. Nowotarski, Phys. Rev. A **98**, 022132 (2018).

[16] A. Fonseca, A. de Rosier, T. Vértesi, W. Laskowski, and F. Parisio, Phys. Rev. A **98**, 042105 (2018).

[17] A. Barasiński, I. I. Arkhipov, and J. Svozilík, Sci. Rep. **8**, 15209 (2018).

[18] A. Barasiński and J. Svozilík, Phys. Rev. A **99**, 012306 (2019).

[19] A. Barasiński, A. Černoch, and K. Lemr, Phys. Rev. Lett. **122**, 170501 (2019).

[20] G. Svetlichny, Phys. Rev. D **35**, 3066 (1987).

[21] J.-D. Bancal, N. Brunner, N. Gisin, and Y.-C. Liang, Phys. Rev. Lett. **106**, 020405 (2011).

[22] J.-D. Bancal, J. Barrett, N. Gisin, and S. Pironio, Phys. Rev. A **88**, 014102 (2013).

[23] F. J. Curchod, M. L. Almeida, and A. Acín, New J. Phys. **21**, 023016 (2019).

[24] J. F. Clauser, M. A. Horne, A. Shimony, and R. A. Holt, Phys. Rev. Lett. **23**, 880 (1969).

[25] F. J. Curchod, Y.-C. Liang, and N. Gisin, J. Phys. A: Math. Theor. **47**, 424014 (2014).

[26] F. J. Curchod, N. Gisin, and Y.-C. Y.-C. Liang, Phys. Rev. A **91**, 012121 (2015).

[27] J. Lavoie, R. Kaltenbaek, and K. J. Resch, New J. Phys. **11**, 073051 (2009).

[28] H.-X. Lu, J.-Q. Zhao, X.-Q. Wang, and L.-Z. Cao, Phys. Rev. A **84**, 012111 (2011).

[29] H.-X. Lu, J.-Q. Zhao, L.-Z. Cao, and X.-Q. Wang, Phys. Rev. A **84**, 044101 (2011).

[30] A. Barasiński, A. Černoch, K. Lemr, and J. Soubusta, Phys. Rev. A **99**, 042123 (2019).

[31] I. Pitowsky, *Quantum Probability – Quantum Logic*, Vol. 321 (Springer-Verlag, Berlin, 1989).

[32] I. Pitowsky and K. Svozil, Phys. Rev. A **64**, 014102 (2001).

[33] C. Śliwa, Phys. Lett. A **317**, 165 (2003).

[34] D. Collins and N. Gisin, J. Phys. A **37**, 1775 (2004).

[35] K. Życzkowski and M. Kuś, J. Phys. A **27**, 4235 (1994).

[36] B. F. Toner and D. Bacon, Phys. Rev. Lett. **91**, 187904 (2003).

[37] S. Ghose, N. Sinclair, S. Debnath, P. Rungta, and R. Stock, Phys. Rev. Lett. **102**, 250404 (2009).

[38] A. Barasiński, Sci. Rep. **8**, 12305 (2018).

[39] C. Eltschka and J. Siewert, J. Phys. A: Math. Theor. **47**, 424005 (2014).

[40] B. Paul, K. Mukherjee, and D. Sarkar, Phys. Rev. A **94**, 032101 (2016).

[41] Z.-H. Ma, Z.-H. Chen, J.-L. Chen, C. Spengler, A. Gabriel, and M. Huber, Phys. Rev. A **83**, 062325 (2011).

[42] J.-L. Chen, C. Wu, L. C. Kwek, C. H. Oh, and M.-L. Ge, Phys. Rev. A **74**, 032106 (2006).

[43] S. Zohren and R. D. Gill, Phys. Rev. Lett. **100**, 120406 (2008).

[44] D. Collins, N. Gisin, N. Linden, S. Massar, and S. Popescu, Phys. Rev. Lett. **88**, 040404 (2002).

[45] P. G. Kwiat, E. Waks, A. G. White, I. Appelbaum, and P. H. Eberhard, Phys. Rev. A **60**, R773 (1999).

[46] A. G. White, D. F. V. James, P. H. Eberhard, and P. G. Kwiat, Phys. Rev. Lett. **83**, 3103 (1999).

[47] E. Halenková, A. Černoch, K. Lemr, J. Soubusta, and S. Drusová, Appl. Opt. **51**, 474 (2012).

[48] http://www.wcss.pl.